Multivariate association between single-nucleotide polymorphisms in Alzgene linkage regions and structural changes in the brain: discovery, refinement and validation

Elena Szefer[1], Donghuan Lu[1], Farouk Nathoo[2], Mirza Faisal Beg[1], Jinko Graham[1] for the Alzheimer's Disease Neuroimaging Initiative[*]

Abstract

Both genetic variants and brain region abnormalities are recognized to play a role in cognitive decline. We explore the association between single-nucleotide polymorphisms (SNPs) in linkage regions for Alzheimer's disease and rates of decline in brain structure using data from the Alzheimer's Disease Neuroimaging Initiative (ADNI).

In an initial discovery stage, we assessed the presence of linear association between the minor allele counts of 75,845 SNPs in the Alzgene linkage regions and estimated rates of change in structural MRI measurements for 56 brain regions using an RV test. In a second, refinement stage, we reduced the number of SNPs using a bootstrap-enhanced sparse canonical correlation analysis (SCCA) with a fixed tuning parameter. Each SNP was assigned an importance measure proportional to the number of times it was estimated to have a nonzero coefficient in repeated re-sampling from the ADNI-1 sample. We created refined lists of SNPs based on importance probabilities greater than 50% and 90%, respectively. In a third, validation stage, we assessed the multivariate association between these refined lists of SNPs and the rates of structural change in an independent dataset comprised of the ADNIGO and ADNI-2 study samples.

There was strong statistical evidence for linear association between the SNPs in the Alzgene linkage regions and the 56 imaging phenotypes in both the ADNI-1 and ADNIGO/2 samples ($p < 0.0001$). The bootstrap-enhanced SCCA identified 1,694 priority SNPs with importance probabilities $> 50\%$ and 22 SNPs with importance probabilities $> 90\%$. The 1,694 prioritized SNPs were associated with imaging phenotypes in the ADNI-1 data ($p < 0.001$) and this association was replicated in the ADNIGO/2 data ($p = 0.0021$).

This manuscript presents an analysis that addresses challenges in current imaging genetics studies such as biased sampling designs, high-dimensional data with low-signal, and

[1]Simon Fraser University, Burnaby, BC, Canada

[2]University of Victoria, Victoria, BC, Canada

[*]Data used in preparation of this article were obtained from the Alzheimer's Disease Neuroimaging Initiative (ADNI) database (adni.loni.usc.edu). As such, the investigators within the ADNI contributed to the design and implementation of ADNI and/or provided data but did not participate in analysis or writing of this report. A complete listing of ADNI investigators can be found at: `http://adni.loni.usc.edu/wp-content/uploads/how_to_apply/ADNI_Acknowledgement_List.pdf`

discovery and validation of association in multivariate analysis. Genes corresponding to priority SNPs having the highest contribution to the RV coefficient test statistic in the validation data have previously been implicated or hypothesized to be implicated in AD, including GCLC, IDE, and STAMBP1andFAS. We hypothesize that the effect sizes of the 1,694 SNPs in the priority set are likely small, but further investigation within this set may advance understanding of the missing heritability in late-onset Alzheimer's disease.

Keywords: Alzheimer's Disease Neuroimaging Initiative; Multivariate analysis; Linkage regions; Imaging genetics; Endophenotypes; Inverse probability weighting; Variable importance probabilities

---

1. Introduction

Alzheimer's disease (AD) is a neurodegenerative disorder causing cognitive impairment and memory loss. The estimated heritability of late-onset AD is 60%-80% (Gatz et al. 2006), and the largest susceptibility allele is the $\varepsilon 4$ allele of *APOE* (Corder et al. 1993), which may play a role in 20% to 25% of AD cases. Numerous studies have identified susceptibility genes which account for some of the missing heritability of AD, with many associated variants having been identified through genome-wide association studies (GWAS) (Beecham et al. 2009) (Kamboh et al. 2012) (Bertram et al. 2008). Apart from *APOE*, the associated variants have mostly had moderate or small effect sizes, suggesting that the remaining heritability of AD may be explained by many additional genetic variants of small effect.

Identifying susceptibility variants with small effect sizes in GWAS is challenging since strict multiple testing corrections are required to maintain a reasonable family-wise error rate. This analysis focuses on leveraging information from prior family of studies of AD (Hamshere et al. 2007) (Butler et al. 2009), by looking for association in previously identified linkage regions reported on the Alzgene website (Biomedical Research Forum 2013). Linkage regions for AD are genomic regions that tend to be co-inherited with AD in families. By definition, linkage regions include susceptibility genes that are co-transmitted with the disease. The regions currently identified from family studies of AD are large, however, since families contain relatively few transmissions. Further transmissions over multiple generations would provide more fine-grain information about the location of susceptibility genes. Previous studies have fine-mapped a single linkage region through association of AD with genetic variants in densely genotyped or sequenced regions ((Fallin et al. 2010) (Ertekin-Taner 2003) (Scott et al. 2000) (Züchner et al. 2008)), or have confirmed linkage to AD in genomic regions identified from GWAS (Anna et al. 2011) . In this report, we aim to fine-map multiple linkage regions for AD through multivariate association of their SNPs to the rates of atrophy in brain regions affected by AD.

We analyze data from the Alzheimer's Disease Neuroimaging Initiative (Mueller et al. 2005), a case-control study of AD and mild-cognitive impairment. The rates of atrophy in brain regions affected by AD are so-called endophenotypes: observable traits that reflect disease progression. By investigating the joint association between the genomic variants and the neuroimaging endophenotypes, higher-resolution information about disease progression

is used to supervise the selection of genomic variants such as single-nucleotide polymorphisms (SNPs). This multivariate approach to analysis stands in contrast to the commonly-used mass-univariate approach in which separate regressions are fit for each SNP, and the disease outcome is predicted by the minor allele counts. Simultaneous analysis of association is preferred because the reduced residual variation leads to (i) a clearer assessment of the signal from each SNP, (ii) increased power to detect signal, and (iii) a decreased false-positive rate (Hoggart et al. 2008). We also employ inverse probability weighting to account for the biased sampling design of the ADNI-1 and ADNIGO/2 studies, an aspect of analysis that has not been accounted for in many previous imaging genetics studies (Zhu et al. 2016).

Methods that explicitly account for gene structure have been proposed for analyzing the association between multiple imaging phenotypes and SNPs in candidate genes (e.g., (Wang et al. 2011) (Greenlaw et al. 2016)). However, these methods become computationally intractable when analyzing data with tens of thousands of genotyped variants. To select SNPs associated with disease progression, we instead use sparse canonical correlation analysis (SCCA) to find a sparse linear combinations of SNPs having maximal correlation with the imaging endophenotypes. Multiple penalty schemes have been proposed to implement the sparse estimation in SCCA (Parkhomenko et al. 2009) (Witten et al. 2009) (Lykou and Whittaker 2010). We employ an SCCA implementation that estimates the sparse linear combinations by computing sparse approximations to the left singular vectors of the cross-correlation matrix of the SNP data and the neuroimaging endophenotype data (Parkhomenko et al. 2009). Sparsity is introduced through soft-thresholding of the coefficient estimates (Donoho and Johnstone 1994), which has been noted (Chalise and Fridley 2012) to be similar in implementation to a limiting form of the elastic-net (Zou and Hastie 2005). We prefer an elastic-net-like penalty over alternative implementations with ℓ_1 penalties because it allows selection of all potentially associated SNPs regardless of the linkage-disequilibrium (LD) structure in the data. A drawback of ℓ_1-type penalties is that not all SNPs from an LD block of highly-correlated SNPs that are associated with the outcome will be selected into the model (Zou and Hastie 2005).

We may think of SNP genotypes as a matrix X and imaging phenotypes as a matrix Y measured on the same n subjects. (Robert and Escoufier 1976) showed that estimating the maximum correlation between linear combinations of X and Y in canonical correlation analysis is equivalent to estimating the linear combinations having the maximum RV coefficient, a measure of linear association between the multivariate datasets (Escoufier 1973). The RV coefficient is therefore well-suited for testing linear association in our context. We use a permutation test based on the RV coefficient to assess the association between the initial list of SNPs in X and the phenotypes in Y. Although the RV coefficient may overestimate association when $n \ll p$ (Smilde et al. 2008), a permutation test with the RV coefficient is preferred over a parametric hypothesis test since the permutation null distribution is computed under the same conditions as the observed RV coefficient, resulting in a valid hypothesis test. The outcome of this test is used to determine whether or not to proceed with a second refinement stage that reduces the number of SNPs by applying SCCA.

Selection of the soft-thresholding parameter in SCCA is challenging in our context. Since the number of SNPs exceeds the sample size and many of the SNPs are expected to be unas-

sociated with the phenotypes, large sample correlations can arise by chance (Fan et al. 2011). Indeed, the prescribed procedure of selecting the penalty parameter with highest predicted correlation across cross-validation test sets (Parkhomenko et al. 2009) results in more than 98% of the SNPs remaining in the model. A prediction criterion for choosing the penalty term may contribute to the lack of variable selection, allowing redundant variables into the model (Leng et al. 2006). When the same tuning parameter is used for variable selection and shrinkage, redundant variables tend to be selected to compensate for overshrinkage of coefficient estimates and losses in predictive ability (Radchenko and James 2008). In our case, there is effectively no variable selection and little insight is gained by allowing for sparsity in the solution. To circumvent the lack of variable selection from SCCA, we fix the tuning parameter to select about 10% of the SNPs (Wu et al. 2009) and then use resampling to determine the relative importance of each SNP to the association with neuroimaging endophenotypes.

The organization of the manuscript is as follows. The Materials and Methods section describes the ADNI data, the data processing procedures, and the methods applied for discovery, refinement, and validation. The Results section presents the results of the analyses. The Discussion section notes challenges and successes of the analysis, including considerations for modelling continuous phenotype data under a case-control sampling design, and provides interpretation of the results.

2. Materials and Methods

2.1. Data

Data used in the preparation of this article were obtained from the Alzheimer's Disease Neuroimaging Initiative (ADNI) database (adni.loni.usc.edu). The ADNI was launched in 2003 as a public-private partnership, led by Principal Investigator Michael W. Weiner, MD. The primary goal of ADNI has been to test whether serial magnetic resonance imaging (MRI), positron emission tomography (PET), other biological markers, and clinical and neuropsychological assessment can be combined to measure the progression of mild cognitive impairment (MCI) and early Alzheimer's disease (AD).

Imaging data. The neuroimaging phenotypes analyzed are estimates of the rates of change in cortical thickness and volumetric measurements in brain regions obtained from magnetic resonance imaging (MRI) scans. ADNI subjects had 1.5 T MRI scans at either 6 or 12 month intervals during the two- to three-year follow-up period of the study and we chose to analyse the longitudinal information on cortical thickness and regional volumes. While other studies have compared the different study groups using imaging information from baseline (Shen et al. 2010)(Meda et al. 2012), the longitudinal information provides insight into the different rates of brain deterioration experienced by people with negligible memory loss compared to those with more acute memory difficulties and Alzheimer's disease.

The MRIs were segmented using Freesurfer (Fischl 2012). For each hemisphere, the 28 volumetric and cortical thickness measurements used for analysis by Shen (Shen et al. 2010) were obtained via automated parcellation of the segmented images in Freesurfer.

Genomic data. The ADNI-1 subjects were genotyped with the Illumina Human610-Quad BeadChip and the ADNIGO/2 subjects were genotyped with the Illumina HumanOmniExpress BeadChip, both of which interrogate SNPs. All genotyping information was downloaded from the LONI Image Data Archive (missing citation). Pre-packaged PLINK (Purcell et al. 2007) files included genotyping information for 757 of the 818 ADNI-1 subjects. Genotyping information for 793 of the ADNIGO/2 subjects were converted from CSV files to PLINK binary files using a publicly-available conversion script (Hibar 2014). The Human610-Quad BeadChip and HumanOmniExpress BeadChip interrogated 620,901 and 730,525 SNPs respectively. APOE was genotyped separately at study screening from DNA extracted from a blood sample.

Inclusion criteria. Subjects were included if their genotyping data was available, if they had a baseline MRI scan, and they had at least one additional follow-up baseline scan. Of the 757 ADNI-1 subjects and 793 ADNIGO/2 subjects with SNP data available, 696 and 583 had both a baseline scan and at least one additional follow-up scan, respectively. Genomic quality control outlined in the Data Processing section was also employed, widening the exclusion criteria, to obtain a more homogeneous sample.

Genomic imputation. Imputation serves two key roles in the analysis: to preserve the sample size for the multivariate analysis by replacing sporadically missing genotypes with imputed ones, and to impute SNPs not interrogated on the ADNIGO/2 chip that are interrogated on the ADNI-1 chip. SNPs were imputed in the ADNI-1 and ADNIGO/2 sample using the HapMap3 panel with NCBI build 36/hg18 using IMPUTE2 (Marchini and Howie 2010), based on the imputation protocol in the IMPUTE2: 1000 Genomes Imputation Cookbook (Luan et al.). Haplotypes were phased with SHAPEIT (Delaneau et al. 2013), and file conversions between PLINK file formats and SHAPEIT/IMPUTE2 formats was accomplished with GTOOL (Freeman 2007–2012). Of the 503,450 SNPs that passed quality control in the ADNI-1 sample, 459,517 were also in the reference panel and had sporadically missing genotypes imputed. Out of the 574,730 SNPs that passed quality control in the ADNIGO/2 sample, sporadically missing genotypes were imputed at the 270,074 SNPs that were also on the ADNI-1 chip and in the reference panel. The remaining 189,443 SNPs that were not genotyped in the ADNIGO/2 sample, but were in both the ADNI-1 sample and the reference panel, were imputed into the sample. The genotyping rate in the imputed data for the ADNIGO/2 sample was 98.2%, prior to filtering out SNPs that have an IMPUTE2 info metric less than 0.5.

Alzgene linkage regions. To focus the analysis on regions that are likely to contain causal genetic variation, SNPs were included in the analysis if they fell in the linkage regions reported by approximate physical position on the Alzgene website (Bertram et al. 2007) (Biomedical Research Forum 2013). These linkage regions have been identified in meta-analyses of family-based studies of Alzheimer's disease (Hamshere et al. 2007) (Butler et al. 2009). A total of 75,845 SNPs from nine chromosomes were included in the analysis from the ADNI-1 sample. Table 2.1 shows the number of SNPs in the ADNI-1 sample that fall

Chromosome	Band	Mb	N
1	p31.1-q31.1	83-185	12005
3	q12.3-q25.31	103-173	10689
6	p21.1-q15	43-91	6785
7	pter-q21.11	0-78	13292
8	p22-p21.1	13-28	4149
9	p22.3-p13.3	20-35	2868
9	q21.31-q32	80-100	3483
10	p14-q24	10-100	15274
17	q24.3-qter	67-79	2319
19	p13.3-qter	8-54	4981

Table 1: The chromosome, band, and location on the Mb scale of the linkage regions of interest. N denotes the number of SNPs in the ADNI-1 data that fall in each linkage region.

in each linkage region. After filtering SNPs that had an IMPUTE2 info metric less than or equal to 0.5, 75,818 SNPs remained in the ADNIGO/2 sample.

Estimating rates of change. Linear mixed effect models, given in Equation 1, were used to estimate the rates of change in each brain region of interest (ROI). A separate mixed model was fit for each ROI, with random effects for subject-specific rates of change and fixed effects for average rates of change within diagnostic subgroups. In the specification of the model, fixed-effects terms are denoted by β, while random-effect terms are denoted by γ. The predictors are (i) t, the time of the follow-up visit at which the scan was conducted, with $t \in 0, 6, 12, 18, 24$ months; (ii) MCI, a dummy variable equal to 1 if subject i has late mild cognitive impairment, and equal to 0 otherwise; and (iii) AD, a dummy variable equal to 1 if subject i has Alzheimer's disease, and equal to 1 otherwise. The ROI's are indexed by j:

$$Y_{ijt} = \beta_{0j} + \beta_{1j}MCI + \beta_{2j}AD + \beta_{3j}t + \beta_{4j}MCI \times t + \beta_{5j}AD \times t + \gamma_{1ij} + \gamma_{2ij}t + \varepsilon_{ijt} \quad (1)$$

The estimated rate of change over the study period for subject i at ROI j is the sum of the disease-specific estimated rate of change and the subject-specific estimated rate of change $\hat{\beta}_{3j} + \hat{\beta}_{4j}MCI + \hat{\beta}_{5j}AD + \hat{\gamma}_{2ij}$. Figure 1 is a heatmap of the estimated rates of change, adjusted for confounding variables as discussed next, in the sample. The heatmap illustrates how decreases in cortical thickness are more pronounced for subjects with AD, and similarly that the ventricles, cavities in the brain filled with cerebrospinal fluid, expand more for subjects with more advanced disease.

Adjustments for confounding. Covariate information cannot be explicitly included in SCCA, so both the imaging and genomic data are adjusted for confounding variables in advance. Potential confounders in the analysis are population stratification and APOE genotype. Population stratification is the phenomenon of systematic differences in allele frequencies in a subpopulation arising because of differences in ancestry, while the $\varepsilon 4$ allele of APOE is

the largest known genetic risk factor for Alzheimer's disease (Corder et al. 1993). Since true population structure is not observed, a set of principal coordinates from multidimensional scaling are used to derive proxy variables for population stratification in the data. We also adjust for APOE genotype as a precautionary measure, since it can account for the population stratification in the data, over and above the principal components or principal coordinates (Lucotte et al. 1997).

Ten principal coordinates for each of the ADNI-1 and ADNIGO/2 datasets were obtained using ten-dimensional multi-dimensional scaling on the pairwise IBS distance matrix, computed with PLINK from 121,795 and 118,012 approximately uncorrelated SNPs from the SNPs that passed quality control filters. The SNP genotypes used to estimate the principal coordinates were from the complete imputed data. The number of principal coordinate dimensions was chosen to follow a similar protocol for adjustment for population stratification using principal components, in which ten axes of variation are suggested (Price et al. 2006).

The data for analysis were obtained by adjusting the minor allele counts and estimated rates of change of the brain ROIs for the ten principal coordinates, as well as for dummy variables for APOE genotype, using weighted ordinary least squares regression. The weights account for certain diagnostic subgroups being over-represented in the sample relative to their population frequency. The residuals from each regression comprised the genomic (X) and neuroimaging (Y) features analyzed.

2.2. Methods

2.2.1. Discovery

Weighted RV test. We tested the analysis dataset, ADNI-1, for linear association between the genomic data and the neuroimaging data. The RV coefficient (Escoufier 1973) is a multivariate generalization of Pearson's r^2 and quantifies the association between the columns of X, or the genotypes, and the columns of Y, the imaging endophenotypes. As the test statistic, we used a weighted version (Omelka and Šárka Hudecová 2013), in which individual contributions are proportional to their inverse probability weight. A permutation test with P=10,000 permutations was used to assess the evidence for association between X and Y.

2.2.2. Refinement

SCCA and resampling. To obtain a sparse linear combination of the SNP genotypes that is most associated with a non-sparse linear combination of the imaging phenotypes, we used sparse canonical correlation analysis (SCCA; (Parkhomenko et al. 2009)), a penalized version of canonical correlation analysis. Sparse linear combinations contain some coefficients which are zero; e.g., in penalized regression analysis, the predicted value is potentially a sparse linear combination of the predictors. SCCA is a multivariate method for estimating maximally correlated sparse linear combinations of the columns of two multivariate datasets collected on the same n subjects, X and Y. We initially applied SCCA to identify a sparse set of SNPs associated with the imaging endophenotypes. Ten-fold cross validation was used to select the penalty parameter for the SNPs, λ_u, to use in SCCA. A search grid for λ_u was defined as $\{0, 10^{-4}, \ldots, 10^{-1}\}$ with the values in the search grid being incremented

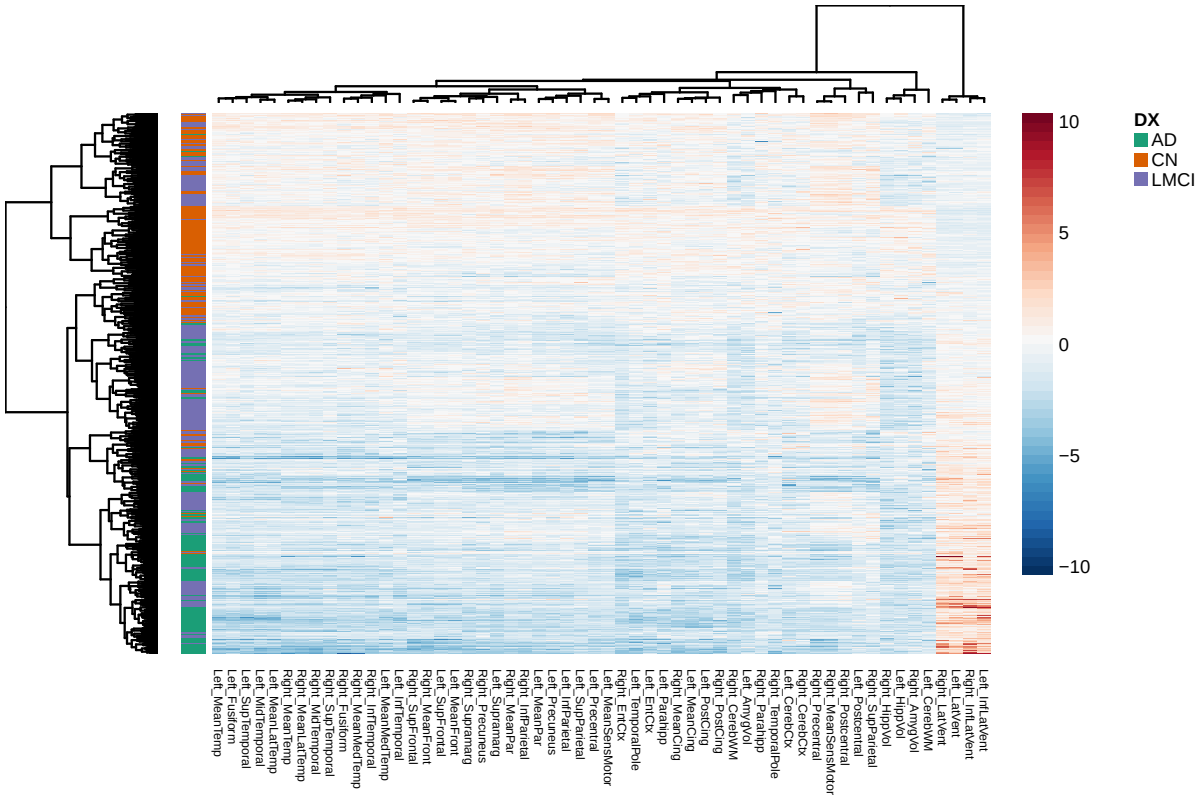

Figure 1: Heatmap of the neuroimaging phenotypes, clustered by similarity among ROIs and subjects. Each row corresponds to a subject in the sample and each column corresponds to one of the 56 ROIs. The rows are annotated by the disease group of the subject. The adjusted, estimated rates of change are shown for each region, where blue values indicate decreases in the volume of thickness in the brain region, and orange values indicate increases in the volume of the brain region. Values for the ventricles clustered on the far right, have an inverted relationships compared to the other ROIs since the ventricles are cavities in the brain which expand as brain atrophy progresses. The thickness of grey matter, by contrast, decreases with atrophy.

by 0.0005. At the ith element in the search grid, $\lambda_{u,i}$, the sparse canonical correlation coefficients were computed in training set j, where the sparse canonical correlation coefficients at grid point i in cross-validation fold j for the SNPs are denoted by $a_{i,j}$, and the coefficients for the endophenotypes are denoted by $b_{i,j}$. The fitted coefficients from the training sets were then used to compute the predicted sample correlation coefficient in each test set: $\hat{r}_{i,j} = Corr(a_{i,j}X_{test_j}, b_{i,j}Y_{test_j})$. The SNP penalty parameter λ_u was chosen as the element in the search grid that maximized the sum of the predicted sample correlation coefficients over the ten test sets. Under this cross-validation scheme, variable selection of the SNPs was minimal with more than 98% of the SNPs remaining in the active set. Ruling out fewer than 2% of the SNPs in the Alzgene linkage regions is insufficient refinement for our analysis.

Instead, we chose to incorporate bootstrap resampling to estimate the relative importance of each SNP in the multivariate association. This approach of "bootstrap enhancement" has been applied previously in neuro-imaging studies (Bunea et al. 2011), to guide variable selection with the elastic-net and the lasso. We obtained B=100,000 bootstrap samples by sampling with replacement within each disease category. The weighted cross-correlation matrix $S_{XY}^{(W)}$ was computed for each bootstrap sample b, and a sparse linear combination of the genomic markers was estimated, using the SCCA penalty parameter $\lambda_u^* = 0.012$ for soft-thresholding the SNP coefficients. A value of $\lambda_u^* = 0.012$ was chosen so that approximately 10% of the SNPs had non-zero estimated coefficients. If $\boldsymbol{\beta}_b = (\beta_{1b}, \beta_{2b}, \ldots, \beta_{pb})$ denotes the coefficient vector of the sparse linear combination of the p SNPs, from bootstrap sample b, then the importance probability for SNP k is defined in equation 2 as the proportion of bootstrap samples in which SNP k ($k = 1, \ldots, p$) has a nonzero coefficient, or is "selected":

$$VIP_k = \frac{1}{B}\sum_{b=1}^{B} \mathbb{I}(\hat{\beta}_{\mathrm{kb}} \neq 0), \text{ where } \mathbb{I}(\mathrm{A}) = 1 \text{ if condition } A \text{ holds and 0 otherwise} \qquad (2)$$

Gene-Set Analysis. To reduce the initial list of 75,845 SNPs to a shorter list for validation and to gain insight into the biologically related sets of genes associated with cognitive decline, we applied a gene-set analysis, as implemented in GSA-SNP (Nam et al. 2010). GSA-SNP combines the evidence for SNP-specific associations into gene-level summaries and assesses the pattern of association for genes in a given set, such as a functional pathway, relative to genes outside the set. We used variable exclusion probabilities, $VEP = 1 - VIP$, to quantify the SNP-specific evidence of association, and the second smallest VEP for SNPs in a gene as the gene-level summary statistic. The re-standardized version of GSA-SNP with the maxmean statistic (Efron and Tibshirani 2007) was applied, with default gene padding of 20000 base pairs and Gene Ontology gene sets. We took $P = 100$ samples under the permutation null hypothesis of no association to serve as the empirical reference distribution for VEPs from ADNI-1. To ensure inclusive selection of SNPs, candidate gene sets were identified by Benjamini-Hochberg corrected p-values with a liberal false discovery rate threshold of 0.8.

2.2.3. Validation

Validation. Two subsets of the SNPs in the Alzgene linkage regions, with estimated importance probabilities $\geq$ 50% and 90%, were used for validation in the ADNIGO/2 sample. The cut-off values were chosen to reflect a relatively liberal and stringent criterion, respectively. We first assessed the evidence for linear association between the top SNPs and all the imaging phenotypes in the ADNIGO/2 validation sample. We then returned to the original ADNI-1 training sample and checked the evidence for association of the reduced list of SNPs there as well. The RV-test with 1,000 permutation replicates was applied in all cases.

Inverse probability weights. To account for the biased sampling in the ADNI-1 and ADNIGO/2 case-control studies, we estimated inverse probability weights for each subject(Horvitz and Thompson 1952). As subjects with early MCI were excluded from ADNI-1, we defined

Sample	n_{CN}	n_{LMCI}	n_{AD}	n
ADNI-1	179	296	157	632
ADNIGO/2	116	104	45	265

Table 2: The number of subjects, n_D, from each disease group D that were analyzed in each study. The total number of subjects analysed in each study is denoted by n.

the target population to be non-Hispanic, white Americans and Canadians aged 55-90 years who are cognitively normal or have been diagnosed with late MCI or Alzheimer's disease.

The Alzheimer's Association reports that 5.2 million Americans had Alzheimer's disease in 2014 (Alzheimer's Association 2014). Additionally, data from the US census in 2010 (U.S. Census Bureau 2011) indicates that approximately 23% of the American population is over the age of 55 and that the total population is 308 million people. Based on this information, the approximate proportion of the American population aged 55-90 years with Alzheimer's disease is $p_{AD} = 7.5\%$, rounded to the nearest half percent. This calculation assumes that individuals aged 90 or more years and patients diagnosed with early MCI represent negligible proportions of the population. We used a late MCI prevalence estimate of $p_{LMCI} = 5\%$ based on an urban study of people aged 65+ in New York (Manly et al. 2005), and assumed that the remaining $p_{CN} = 87.5\%$ of the population of interest is cognitively normal.

A breakdown of the number of subjects used in the analysis by study is given in Table 2.2.3.

The inverse probability weights $w_{DX,sample}$ for each disease group and sample are computed as the assumed prevalence of the disease in the target population divided by the number of subjects sampled from the disease group; for example,

$$w_{AD,ADNI-1} = \frac{p_{AD}}{n_{AD,ADNI-1}}. \tag{3}$$

The weights are standardized to sum to 1.

3. Results

3.1. Discovery

The RV-test in the ADNI-1 data rejected the null hypothesis of no linear association between X and Y. The observed RV coefficient was $RV = 0.079$, and the permutation test p-value was $p < 0.001$.

3.2. Refinement

The resampling procedure coupled with SCCA in the ADNI-1 data produces variable importance probabilities (VIPs) for each SNP in the Alzgene linkage regions. Figure 2 is a Manhattan-like plot of the variable exclusion probabilities, $VEP = 1 - VIP$, plotted on the $-\log_{10}$ scale, such that SNPs with $VIP \geq 0.9$, have values of $-\log_{10}(VEP) \geq 1$. The dotted reference line indicates the $VIP = 0.5$ cut-off used to identify the priority SNPs.

. 1,694 SNPs had $VIP > 0.5$, a set of reduced SNPs we call the priority set. As expected, the priority SNPs, $X_{reduced}$, were associated with the endophenotypes in the ADNI-1 training data, based on a permutation RV test ($RV = 0.23$, $p < 0.001$). Using the stringent cut-off of $VIP > 0.9$ for SNP selection, 22 SNPs were included in a set of SNPs we call the set of top-hits. As expected, the top-hit SNPs, X_{top}, were also associated with the endophenotypes in the ADNI-1 training data ($p < 0.001$). There was no evidence of enrichment in biological pathways based on results from GSA-SNP.

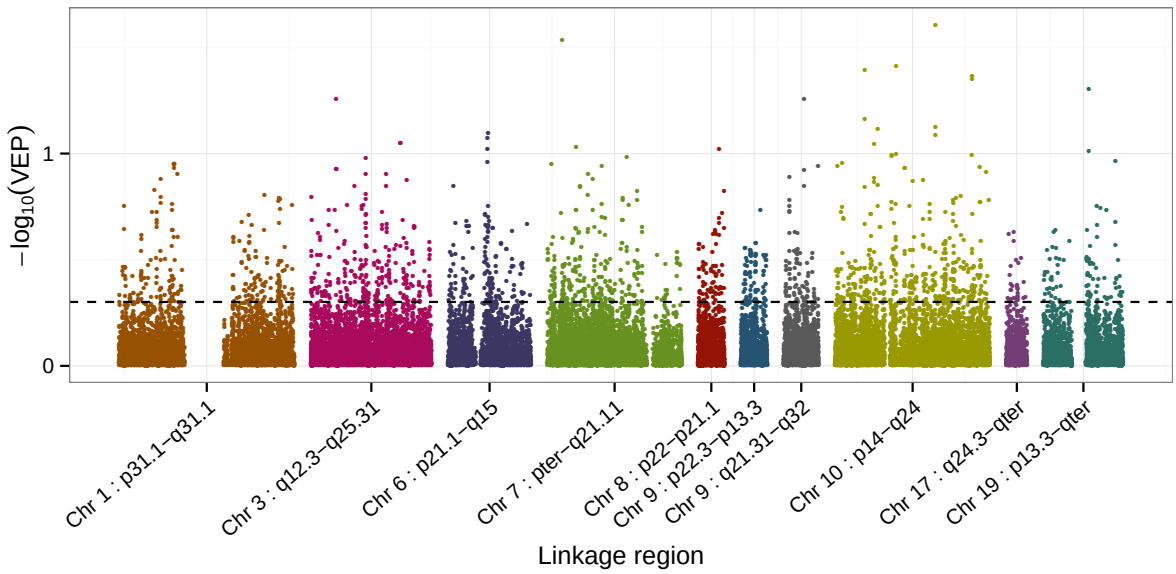

Figure 2: Plot of the $-\log_{10}(VEP)$ of the SNPs in each of the Alzgene linkage regions. The dotted reference line indicates the $VIP = 0.5$ cut-off used to define the priority set of SNPs $X_{reduced}$.

. Figure 2 shows that very few SNPs had $VIP \geq 0.9$, as evidenced by the sparse selection of SNPs with $-\log_{10}(VEP) \geq 1$ in the plot. While the linkage region on chromosome 10 is the largest, it also has the most SNPs with $VIP \geq 0.9$ and its SNPs have relatively high inclusion probabilities across the entire linkage region, in contrast to the linkage region from chromosome 6, for example. The smaller linkage regions p22.3-p-13.3 on chromosome 9 and q24.3-qter on chromosome 17 have relatively low inclusion probabilities, overall.

3.3. Validation

. Let $X^*_{reduced}$ and X^*_{top} be the ADNIGO/2 validation data at the priority and top-hit sets of SNPs, respectively, and let Y^* be the validation endophenotype data. We were able to validate our finding of association between the priority set of SNPs and the endophenotypes in the ADNIGO/2 data. The RV test of association between $X^*_{reduced}$ and Y^* had an observed test statistic of $RV_{obs} = 0.073$, and a permutation p-value of $p = 0.0021$. However, there was no evidence of association between the top-hit set of SNPs and the endophenotypes ($p = 0.79$).

. To further understand the observed association between SNPs in the priority set and endophenotypes in the ADNIGO/2 validation data, we decomposed the RV test statistic into its SNP-specific components. Figure 3 depicts the contribution of each SNP as a score, normalized to have mean 1 over all the SNPs in the priority set. Before normalization, the contribution for SNP i in the priority set is a sum, $\sum_{j=1}^{q} S^2_{X^*_{\text{reduced},i} Y^*_j}$, over the $q = 56$ endophenotypes in the cross-correlation matrix, $S^2_{X^*_{reduced} Y^*}$, from the ADNIGO/2 validation data. Each point in the plot therefore represents the relative contribution of a given SNP to the RV coefficient, summed over the 56 endophenotypes. SNPs with higher relative contributions can be viewed as the SNPs driving the association found in the RV test.

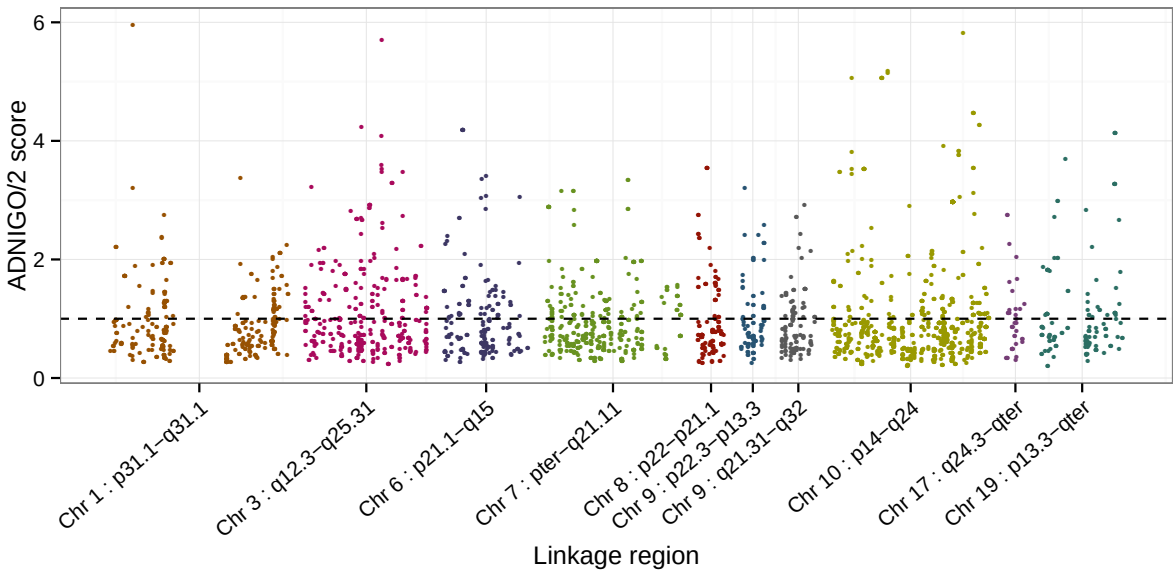

Figure 3: SNP-specific scores at the priority set SNPs in the ADNIGO/2 validation data, with scores defined as described in text. SNPs with higher score contribute relatively more to the RV coefficient between $X^*_{reduced}$ and Y^*. The dashed horizontal reference line corresponds to a score of 1, or the average score for a SNP in the priority set in the ADNIGO/2 validation data.

. Table 3.3 summarizes information about the top 20 scoring SNPs in the priority set, with gene annotations obtained from SNPNexus (Ullah et al. 2012). SNPNexus was queried using assembly NCBI36/hg18, the UCSC genome browser (Speir et al. 2015) and AceView (Thierry-Mieg and Thierry-Mieg 2006). The resulting gene symbols for annotated SNPs are reported in the Genes column of the table. We used the squared Pearson correlation coefficient, r^2, to measure the linkage disequilibrium (LD) between SNPs. Values of r^2 were computed in R (Clayton and Leung 2007) using the $N = 116$ cognitively normal subjects in the ADNIGO/2 data. LD blocks within the priority set are indicated by numbers in the first column of Table 3.3, and are defined such that all SNPs within a block have pairwise r^2 greater than 0.7.

LD block	SNP	score*	CHR	BP	Band	VIP	Genes
	rs17328231	5.96	1	95791119	p31.1-q31.1	0.54	
	rs6439445	4.24	3	135119256	q12.3-q25.31	0.72	
	rs16856619	4.08	3	146493435	q12.3-q25.31	0.58	
	rs345015	5.70	3	146667792	q12.3-q25.31	0.62	
1	rs634364	4.18	6	53575551	p21.1-q15	0.57	AK126334, BC050580, AK125128, GCLC
1	rs525248	4.18	6	53576038	p21.1-q15	0.57	AK126334, BC050580, AK125128
2	rs2148885	3.82	10	21413099	p14-q24	0.57	NEBL
2	rs11012530	5.06	10	21444536	p14-q24	0.58	NEBL
3	rs7897675	5.06	10	38448572	p14-q24	0.55	ZNF37A
3	rs17588142	5.06	10	38467714	p14-q24	0.55	
3	rs7080636	5.06	10	38659180	p14-q24	0.50	
3	rs34350622	5.17	10	41848403	p14-q24	0.51	
	rs12255371	5.15	10	41970728	p14-q24	0.51	
	rs7088870	3.91	10	73723319	p14-q24	0.59	
4	rs7094314	3.83	10	82321942	p14-q24	0.55	SH2D4B
4	rs7904557	3.77	10	82326243	p14-q24	0.56	SH2D4B
	rs12768174	5.82	10	84889167	p14-q24	0.74	
	rs10887866	4.48	10	90661730	p14-q24	0.56	STAMBPL1, KIAA1373, STAMBPL1andFAS
	rs4646957	4.26	10	94219892	p14-q24	0.54	IDE
	rs1235382	4.13	19	49711347	p13.3-qter	0.89	CEACAM20

* SNP-specific score indicating relative contribution to the RV statistic, as defined in text.

Table 3: The 20 SNPs with highest SNPs scores in the ADNIGO/2 dataset. Gene annotation obtained from SNPNexus queried with the UCSC genome browser and AceView. LD blocks comprise blocks of SNPs where all SNPs are in LD with $R^2 > 0.7$.

4. Discussion

. In this report, we have taken a targeted approach to genetic association mapping of Alzheimer's disease by focusing on SNPs in Alzheimer's disease linkage regions and on imaging endophenotypes for brain regions affected by Alzheimer's disease. We discovered association between SNPs in the linkage regions and the imaging endophenotypes, refined the set of SNPs by selecting those with high variable inclusion probabilities, and validated the refined set in an independent dataset. Here, we discuss our observations about the benefits and pitfalls of applying data-integration methods such as sparse canonical correlation analysis and the RV test in a high-dimensional data setting with low signal. We also discuss potential links between Alzheimer's disease and genes in the priority set that were ranked highly in the validation data.

. Initially, SCCA was used to find a subset of the SNPs in the linkage regions associated with the endophenotypes, but very little variable selection was achieved. SCCA uses a prediction criterion to identify the optimal soft-thresholding parameters for the sparse canonical variables, but using prediction error to select the penalty term is well known to include irrelevant variables in the active set (Leng et al. 2006). In addition, the prediction-optimal value of the penalty term does not coincide with model selection consistency (Meinshausen and Bühlmann 2006). Instead of using the prediction-optimal penalty term, we fixed the soft-thresholding parameter for the SNPs to achieve variable selection based on the rationale that no more than about 7,500 SNPs, or approximately (10%), are expected to be associated with the phenotypes. This choice is guided by prior experience in genetic association studies, where the majority of genetic variants have no effect on the phenotypes, or an effect that is indistinguishable from zero (Carbonetto and Stephens 2012). We applied bootstrapped-enhanced SCCA, a procedure analogous to the bootstrapped-enhanced elastic net proposed by (Bunea et al. 2011) for imaging applications in which the number of subjects is few relative to the number of predictor variables. To obtain a reduced set of SNPs to carry forward for validation, we then thresholded the variable inclusion probabilities at 50%, as suggested by these authors, and at 90%. Bootstrapping to aid variable selection has been shown to be consistent in high-dimensional settings under some assumptions (Meinshausen and Bühlmann 2010), and can improve recovery of the true model in regularized regression (Bach 2008).

. We selected 22 "top-hit" SNPs by applying a stringent threshold of $VIP \geq 90\%$ in the ADNI-1 training data. The *post-hoc* association between the "top-hit" SNPs and the neuroimaging endophenotypes in the training data ($p < 0.001$) is expected, since the variable selection and hypothesis test are both computed in-sample. We note that, in a low signal context, the inability to replicate association of the "top-hit" SNPs in the ADNI-GO/2 validation data is not unexpected. For a fixed sample size, as the number of unassociated SNPs increases, the probability of a truly associated SNP being within the top-ranked SNPs decreases (Zaykin 2005). By contrast, the more liberal threshold of $VIP \geq 50\%$ resulted in a larger, "priority" set of 1694 SNPs which could be validated and was substantially refined from the initial list of 75,845. In our context of few subjects relative to SNPs, the selection

of an appropriate threshold for SNP selection is an important open question, since analyses involving tens of thousands of SNPs lend themselves to ranking of SNPs by some measure, be it a p-value from a mass-univariate analysis or a variable importance probability.

. The permutation-based RV test of association proved to be a powerful tool in different phases of the analysis. This nonparametric test was computationally tractable and allowed us to uncover and validate linear association between the two multivariate datasets, one of them very high-dimensional, in an analysis setting with a low signal. Despite the evidence for association, the observed RV coefficient at each of the discovery, refinement and validation stages of the analysis was not large (< 0.1), consistent with SNPs having small association effects. The presence of SNPs with small effects is anticipated, as previous studies have found no large genetic effects apart from *APOE* (Ridge et al. 2013), for which we have already adjusted. While the RV coefficient overestimates similarity between two data matrices when the sample size is small and the data are high-dimensional (Smilde et al. 2008), permutation tests using the RV coefficient as a test-statistic remain valid for detecting association because the permutation null distribution is computed under the same sample size and data dimensions as the observed test statistic.

. While there have been many analyses of the genomic and neuroimaging variation in the ADNI data, the analysis of (Vounou et al. 2012) is similar to our own in that SNPs were refined into a priority subset by variable importance probability. These authors split the ADNI data into three analysis sets: the set of the AD and LMCI subjects, the set of the AD and CN subjects, and the set of the LMCI and CN subjects. In each analysis set, they found neuroimaging signatures that discriminated between subjects in the two diagnosis categories, then used the signatures to supervise selection of associated SNPs in a reduced rank regression. They found that the *APOE* genotype as well as SNPs from the *TOMM40* gene were ranked highly for association with a neuroimaging biomarker that distinguished between subjects with AD and CN. *APOE* is the largest known genetic risk factor for AD, and SNPs in *TOMM40* have been found to be predictive of age of onset of AD (Roses et al. 2009). While their highly ranked genomic variants have been previously implicated with AD, the treatment of each of the analysis sets as representative samples in the reduced rank regression means that the general interpretability of these rankings is lacking. The ADNI studies use a case-control design, in which subjects are sampled conditional on meeting diagnostic criteria for either being cognitively normal, having late MCI, or having AD. Case-control designs do not result in a random sample from the population and they cannot be used to make inference about the population association between SNP genotypes and neuroimaging biomarkers without accounting for the biased sampling. To account for the biased sampling, we have applied inverse probability weighting in our analyses.

. Investigation of the genes associated with the highest scoring SNPs in the validation data, reported in Table 3.3, identified genes previously implicated in AD. On chromosome 6, Glutamate-Cysteine Ligase Catalytic Subunit or *GCLC*, a gene annotation of the SNP rs634364, codes the first, rate-limiting enzyme of glutathione synthesis. Glutathione is an

important antioxidant which plays an integrated role in the regulation of cell life, cell proliferation, and cell death (Pompella et al. 2003). The brain glutathione system is hypothesized to play a role in the breakdown of proteins in the brain, such as Aβ peptides (Lasierra-Cirujeda et al. 2013), and abundance of glutathione decreases with age and in some age-related disease (Liu et al. 2004). On chromosome 10, the complex locus *STAMPBL1andFAS* is an annotation of rs10887866 and codes a protein which plays a central role in programmed cell death (Choi and Benveniste 2004). Through modulation of programmed cell death and neuronal atrophy, FAS may play a role in AD (Erten-Lyons et al. 2010). Also on chromosome 10, the gene insulin degrading enzyme (*IDE*) contains rs4646957 and codes the enzyme of the same name. *IDE* has previously been implicated in the progression Alzheimer's disease as it degrades the Aβ peptides which are the main components in the amyloid plaques on the brains of subjects with Alzheimer's disease (Edland et al. 2003). Edland et. al. found that three *IDE* variants were associated with risk of AD in subjects without copies of the $\varepsilon 4$ *APOE* risk allele, the allele which constitutes the largest genetic risk of AD.

. Gene expression from the UCSC RNA-Seq GTEx track was also explored to determine if any of the genes reported were highly expression in the brain. On chromosome 10, Zinc Finger Protein 37A (*ZNF37A*), the gene containing rs7897675, is most highly expressed in the cerebellum and cerebellar hemisphere of the brain, regions related to motor function. Nebulette (*NEBL*), the gene annotation of rs2148885 and rs11012530, is most highly expressed in the heart, but has next highest gene expression in the brain. In addition, association fine-mapping under a linkage peak identified *NEBL* as a candidate gene for vitamin D levels in the blood (Aslibekyan et al. 2016). Low vitamin D blood levels are associated with accelerated decline in cognitive function in older adults (Miller et al. 2015).

. Ten of the top 20 SNPs in Table 3.3 did not have associated gene annotations in the UCSC genome browser or AceView. For these SNPs, flanking genes were queried with ALFRED (Rajeevan et al. 2011) and the UCSC genome browser, since SNPs may "tag" causal variants in nearby genes. Genes were considered to be flanking if they were within 1 Mb of the SNPs in the priority set, though many of the flanking genes reported are much closer to the priority SNPs. On chromosome 3, rs643944 is approximately 22 kb proximal to the flanking gene *RAB6B*. *RAB6B* is the brain-specific isoform of *RAB6* (Wanschers et al. 2007), a family of proteins which impair the processing of the amyloid precursor protein involved in the development of AD (Thyrock et al. 2013). On chromosome 10, *DDIT4* is approximately 17.5 kb proximal to rs7088870. *DDIT4* produces the REDD1 protein, which enhances stress-dependent neuronal cell death and is involved in dysregulation of the mammalian target of rapamycin (mTOR) pathway (Maiese 2014). Dysregulation of mTOR is a hallmark of a wide variety of brain disorders (Polman et al. 2012), and inhibition of mTOR is associated with Aβ-peptide-related synaptic dysfunction in AD (Ma et al. 2010). Another flanking gene to rs7088870 is *DNAJB12*, which is appoximately 39.2 kb proximal to rs7088870, and is involved in protein folding. The process of plaque build-up in AD involves the accumulation of misfolded Aβ proteins, and *DNAJB12* is highly expressed throughout the brain (Tebbenkamp and Borchelt 2010). Finally, in addition to being the gene annotation of rs7897674, *ZNF37A* is also 15.4 kb proximal to the SNP rs17588142 on chromosome 10.

. In summary, this analysis illustrates the application of novel methods for integration of high-dimensional data with low signal. To focus on regions with increased prior probability of containing deleterious variants, the analysis was restricted to SNPs within linkage regions for AD. The objective was to obtain a refined list of SNPs to propose for further investigation. Naive application of SCCA did not lead to any refinement, potentially due to the data containing many small effects. Instead, we were able to obtain refinement through bootstrapped-enhanced SCCA. Throughout, the analysis benefited from the RV test to assess the evidence of linear association between two multivariate datasets: the high-dimensional genomic data, and the multidimensional neuroimaging data. RV tests of SNPs selected based on variable importance probabilities identified a priority set of 1,694 SNPs in the ADNI1 data that was associated with the rates of changes in the brain regions of interest in the ADNIGO/2 validation set. Our final results are encouraging, in that genes corresponding to SNPs with the highest contributions to the RV coefficient in the validation data have previously been implicated or hypothesized to be implicated in AD, including *GCLC*, *IDE*, and *STAMBP1andFAS*. We hypothesize that the effect sizes of the 1,694 SNPs in the priority set are likely small, but further investigation within this set may advance understanding of the missing heritability in late-onset Alzheimer's disease.

5. Acknowledgements

Data collection and sharing was funded by the Alzheimer's Disease Neuroimaging Initiative (ADNI) (National Institutes of Health Grant U01 AG024904) and DOD ADNI (Department of Defense award number W81XWH-12-2-0012). ADNI is funded by the National Institute on Aging, the National Institute of Biomedical Imaging and Bioengineering, and through generous contributions from the following: AbbVie, Alzheimer's Association; Alzheimer's Drug Discovery Foundation; Araclon Biotech; BioClinica, Inc.; Biogen; Bristol-Myers Squibb Company; CereSpir, Inc.; Eisai Inc.; Elan Pharmaceuticals, Inc.; Eli Lilly and Company; EuroImmun; F. Hoffmann-La Roche Ltd and its affiliated company Genentech, Inc.; Fujirebio; GE Healthcare; IXICO Ltd.; Janssen Alzheimer Immunotherapy Research & Development, LLC.; Johnson & Johnson Pharmaceutical Research & Development LLC.; Lumosity; Lundbeck; Merck & Co., Inc.; Meso Scale Diagnostics, LLC.; NeuroRx Research; Neurotrack Technologies; Novartis Pharmaceuticals Corporation; Pfizer Inc.; Piramal Imaging; Servier; Takeda Pharmaceutical Company; and Transition Therapeutics. The Canadian Institutes of Health Research is providing funds to support ADNI clinical sites in Canada. Private sector contributions are facilitated by the Foundation for the National Institutes of Health (www.fnih.org). The grantee organization is the Northern California Institute for Research and Education, and the study is coordinated by the Alzheimer's Disease Cooperative Study at the University of California, San Diego. ADNI data are disseminated by the Laboratory for Neuro Imaging at the University of Southern California.

This work is based on Elena Szefer's MSc thesis supervised by J Graham and was supported in part by the Natural Sciences and Engineering Research Council of Canada. The authors would like to thank Ellen Wisjman for helpful discussions about *APOE* and population stratification and Wayne Wang for assistance with the genomic quality control of the

ADNIGO/2 validation data.

References

Gatz M, Reynolds CA, Fratiglioni L, and others (2006) Role of Genes and Environments for Explaining Alzheimer Disease. Arch Gen Psychiatry 63:168. doi: 10.1001/archpsyc.63.2.168

Corder E, Saunders A, Strittmatter W, and others (1993) Gene dose of apolipoprotein E type 4 allele and the risk of Alzheimer's disease in late onset families. Science 261:921–923. doi: 10.1126/science.8346443

Beecham GW, Martin ER, Li Y-J, and others (2009) Genome-wide Association Study Implicates a Chromosome 12 Risk Locus for Late-Onset Alzheimer Disease. The American Journal of Human Genetics 84:35–43. doi: 10.1016/j.ajhg.2008.12.008

Kamboh MI, Demirci FY, Wang X, and others (2012) Genome-wide association study of Alzheimer's disease. Translational Psychiatry 2:e117. doi: 10.1038/tp.2012.45

Bertram L, Lange C, Mullin K, and others (2008) Genome-wide Association Analysis Reveals Putative Alzheimer's Disease Susceptibility Loci in Addition to APOE. The American Journal of Human Genetics 83:623–632. doi: 10.1016/j.ajhg.2008.10.008

Hamshere ML, Holmans PA, Avramopoulos D, and others (2007) Genome-wide linkage analysis of 723 affected relative pairs with late-onset Alzheimer's disease. Human Molecular Genetics 16:2703–2712. doi: 10.1093/hmg/ddm224

Butler AW, Ng MYM, Hamshere ML, and others (2009) Meta-analysis of linkage studies for Alzheimer's disease—A web resource. Neurobiology of Aging 30:1037–1047. doi: 10.1016/j.neurobiolaging.2009.03.013

Biomedical Research Forum LLC (2013) ALZGENE - PUTATIVE AD LINKAGE REGIONS BASED ON JOINT ANALYSES BY HAMSHERE ET AL. (2007), AND META-ANALYSES BY BUTLER ET AL. (2009).

Fallin MD, Szymanski M, Wang R, and others (2010) Fine mapping of the chromosome 10q11-q21 linkage region in Alzheimer's disease cases and controls. Neurogenetics 11:335–348. doi: 10.1007/s10048-010-0234-9

Ertekin-Taner N (2003) Fine mapping of the -T catenin gene to a quantitative trait locus on chromosome 10 in late-onset Alzheimer's disease pedigrees. Human Molecular Genetics 12:3133–3143. doi: 10.1093/hmg/ddg343

Scott WK, Grubber JM, Conneally PM, and others (2000) Fine-mapping of the chromosome 12 Alzheimer disease locus using family-based association tests of microsatellite markers. Neurobiology of Aging 21:129. doi: 10.1016/s0197-4580(00)82380-5

Züchner S, Gilbert JR, Martin ER, and others (2008) Linkage and Association Study of Late-Onset Alzheimer Disease Families Linked to 9p21.3. Annals of Human Genetics 72:725–731. doi: 10.1111/j.1469-1809.2008.00474.x

Anna S, Lena L, Charlotte F, and others (2011) Linkage to the 8p21.1 Region Including the CLU Gene in Age at Onset Stratified Alzheimer's Disease Families. Journal of Alzheimer's Disease 23:13–20. doi: 10.3233/JAD-2010-101359

Mueller SG, Weiner MW, Thal LJ, and others (2005) Ways toward an early diagnosis in Alzheimer's disease: The Alzheimer's Disease Neuroimaging Initiative (ADNI). Alzheimer's & Dementia 1:55–66. doi: 10.1016/j.jalz.2005.06.003

Hoggart CJ, Whittaker JC, Iorio MD, Balding DJ (2008) Simultaneous Analysis of All SNPs in Genome-Wide and Re-Sequencing Association Studies. PLoS Genetics 4:e1000130. doi: 10.1371/journal.pgen.1000130

Zhu W, Yuan Y, Zhang J, and others (2016) Genome-wide association analysis of secondary imaging phenotypes from the Alzheimer's disease neuroimaging initiative study. NeuroImage. doi: 10.1016/j.neuroimage.2016.09.055

Wang H, Nie F, Huang H, and others (2011) Identifying quantitative trait loci via group-sparse multitask regression and feature selection: an imaging genetics study of the ADNI cohort. Bioinformatics 28:229–237. doi: 10.1093/bioinformatics/btr649

Greenlaw K, Szefer E, Graham J, and others (2016) A Bayesian Group Sparse Multi-Task Regression Model for Imaging Genetics.

Parkhomenko E, Tritchler D, Beyene J (2009) Sparse Canonical Correlation Analysis with Application to Genomic Data Integration. Statistical Applications in Genetics and Molecular Biology 8:1–34. doi: 10.2202/1544-6115.1406

Witten DM, Tibshirani R, Hastie T (2009) A penalized matrix decomposition with applications to sparse principal components and canonical correlation analysis. Biostatistics 10:515–534. doi: 10.1093/biostatistics/kxp008

Lykou A, Whittaker J (2010) Sparse CCA using a Lasso with positivity constraints. Computational Statistics & Data Analysis 54:3144–3157. doi: 10.1016/j.csda.2009.08.002

Donoho DL, Johnstone JM (1994) Ideal Spatial Adaptation by Wavelet Shrinkage. Biometrika 81:425–455. doi: 10.1093/biomet/81.3.425

Chalise P, Fridley BL (2012) Comparison of penalty functions for sparse canonical correlation analysis. Computational Statistics & Data Analysis 56:245–254. doi: 10.1016/j.csda.2011.07.012

Zou H, Hastie T (2005) Regularization and variable selection via the elastic net. Journal of the Royal Statistical Society: Series B (Statistical Methodology) 67:301–320. doi: 10.1111/j.1467-9868.2005.00503.x

Robert P, Escoufier Y (1976) A Unifying Tool for Linear Multivariate Statistical Methods: The RV- Coefficient. Applied Statistics 25:257. doi: 10.2307/2347233

Escoufier Y (1973) Le Traitement des Variables Vectorielles. Biometrics 29:751. doi: 10.2307/2529140

Smilde AK, Kiers HAL, Bijlsma S, and others (2008) Matrix correlations for high-dimensional data: the modified RV-coefficient. Bioinformatics 25:401–405. doi: 10.1093/bioinformatics/btn634

Fan J, Guo S, Hao N (2011) Variance estimation using refitted cross-validation in ultra-high dimensional regression. Journal of the Royal Statistical Society: Series B (Statistical Methodology) 74:37–65. doi: 10.1111/j.1467-9868.2011.01005.x

Leng C, Lin Y, Wahba G (2006) A note on the lasso and related procedures in model selection. Statistica Sinica 1273–1284.

Radchenko P, James GM (2008) Variable Inclusion and Shrinkage Algorithms. Journal of the American Statistical Association 103:1304–1315. doi: 10.1198/016214508000000481

Wu TT, Chen YF, Hastie T, and others (2009) Genome-wide association analysis by lasso penalized logistic regression. Bioinformatics 25:714–721. doi: 10.1093/bioinformatics/btp041

Shen L, Kim S, Risacher SL, and others (2010) Whole genome association study of brain-wide imaging phenotypes for identifying quantitative trait loci in MCI and AD: A study of the ADNI cohort. NeuroImage 53:1051–1063. doi: 10.1016/j.neuroimage.2010.01.042

Meda SA, Narayanan B, Liu J, and others (2012) A large scale multivariate parallel ICA method reveals novel imaging–genetic relationships for Alzheimer's disease in the ADNI cohort. NeuroImage 60:1608–1621. doi: 10.1016/j.neuroimage.2011.12.076

Fischl B (2012) FreeSurfer. NeuroImage 62:774–781. doi: 10.1016/j.neuroimage.2012.01.021

LONI Image Data Archive.

Purcell S, Neale B, Todd-Brown K, and others (2007) PLINK: A Tool Set for Whole-Genome Association and Population-Based Linkage Analyses. The American Journal of Human Genetics 81:559–575. doi: 10.1086/519795

Hibar D (2014) ADNI_Genetics_Convert_to_PLINK. GitHub repository

Marchini J, Howie B (2010) Genotype imputation for genome-wide association studies. Nat Rev Genet 11:499–511. doi: 10.1038/nrg2796

Luan J, Teumer A, Zhao J-H, and others IMPUTE2: 1000 Genomes Imputation Cookbook.

Delaneau O, Zagury J-F, Marchini J (2013) Improved whole-chromosome phasing for disease and population genetic studies. Nature Methods 10:5–6.

Freeman C (2007–2012) GTOOL.

Bertram L, McQueen MB, Mullin K, and others (2007) Systematic meta-analyses of Alzheimer disease genetic association studies: the AlzGene database. Nature Genetics 39:17–23. doi: 10.1038/ng1934

Lucotte G, Loirat F, Hazout S (1997) Pattern of gradient of apolipoprotein E allele *4 frequencies in western Europe.. Hum Biol 69:253–62.

Price AL, Patterson NJ, Plenge RM, and others (2006) Principal components analysis corrects for stratification in genome-wide association studies. Nature Genetics 38:904–909. doi: 10.1038/ng1847

Omelka M, Šárka Hudecová (2013) A comparison of the Mantel test with a generalised distance covariance test. Environmetrics 24:449–460. doi: 10.1002/env.2238

Bunea F, She Y, Ombao H, and others (2011) Penalized least squares regression methods and applications to neuroimaging. NeuroImage 55:1519–1527. doi: 10.1016/j.neuroimage.2010.12.028

Nam D, Kim J, Kim S-Y, Kim S (2010) GSA-SNP: a general approach for gene set analysis of polymorphisms. Nucleic Acids Research 38:W749–W754. doi: 10.1093/nar/gkq428

Efron B, Tibshirani R (2007) On testing the significance of sets of genes. Ann Appl Stat 1:107–129. doi: 10.1214/07-aoas101

Horvitz DG, Thompson DJ (1952) A Generalization of Sampling Without Replacement from a Finite Universe. Journal of the American Statistical Association 47:663–685. doi: 10.1080/01621459.1952.10483446

Alzheimer's Association (2014) 2014 Alzheimer's disease facts and figures. Alzheimer's & Dementia 10:47–92.

U.S. Census Bureau (2011) Table: Resident Population Data, 2010 Census.

Manly JJ, Bell-McGinty S, Tang M-X, and others (2005) Implementing Diagnostic Criteria and Estimating Frequency of Mild Cognitive Impairment in an Urban Community. Arch Neurol 62:1739. doi: 10.1001/archneur.62.11.1739

Ullah AZD, Lemoine NR, Chelala C (2012) SNPnexus: a web server for functional annotation of novel and publicly known genetic variants (2012 update). Nucleic Acids Research 40:W65–W70. doi: 10.1093/nar/gks364

Speir ML, Zweig AS, Rosenbloom KR, and others (2015) The UCSC Genome Browser database: 2016 update. Cold Spring Harbor Laboratory Press

Thierry-Mieg D, Thierry-Mieg J (2006)Genome Biol 7:S12. doi: 10.1186/gb-2006-7-s1-s12

Clayton D, Leung H-T (2007) An R Package for Analysis of Whole-Genome Association Studies. Human Heredity 64:45–51. doi: 10.1159/000101422

Meinshausen N, Bühlmann P (2006) High-dimensional graphs and variable selection with the Lasso. Ann Statist 34:1436–1462. doi: 10.1214/009053606000000281

Carbonetto P, Stephens M (2012) Scalable Variational Inference for Bayesian Variable Selection in Regression and Its Accuracy in Genetic Association Studies. Bayesian Anal 7:73–108. doi: 10.1214/12-ba703

Meinshausen N, Bühlmann P (2010) Stability selection. Journal of the Royal Statistical Society: Series B (Statistical Methodology) 72:417–473. doi: 10.1111/j.1467-9868.2010.00740.x

Bach FR (2008) Bolasso. In: Proceedings of the 25th international conference on Machine learning - ICML '08. Association for Computing Machinery (ACM),

Zaykin DV (2005) Ranks of Genuine Associations in Whole-Genome Scans. Genetics 171:813–823. doi: 10.1534/genetics.105.044206

Ridge PG, Mukherjee S, Crane PK, Kauwe JSK (2013) Alzheimer's Disease: Analyzing the Missing Heritability. PLoS ONE 8:e79771. doi: 10.1371/journal.pone.0079771

Vounou M, Janousova E, Wolz R, and others (2012) Sparse reduced-rank regression detects genetic associations with voxel-wise longitudinal phenotypes in Alzheimer's disease. NeuroImage 60:700–716. doi: 10.1016/j.neuroimage.2011.12.029

Roses AD, Lutz MW, Amrine-Madsen H, and others (2009) A TOMM40 variable-length polymorphism predicts the age of late-onset Alzheimer's disease. Pharmacogenomics J 10:375–384. doi: 10.1038/tpj.2009.69

Pompella A, Visvikis A, Paolicchi A, and others (2003) The changing faces of glutathione a cellular protagonist. Biochemical Pharmacology 66:1499–1503. doi: 10.1016/s0006-2952(03)00504-5

Lasierra-Cirujeda J, Coronel P, Gimeno M, Aza M (2013) Beta-amyloidolysis and glutathione in Alzheimer's disease. Journal of Blood Medicine 31. doi: 10.2147/jbm.s35496

Liu H, Wang H, Shenvi S, and others (2004) Glutathione Metabolism during Aging and in Alzheimer Disease. Annals of the New York Academy of Sciences 1019:346–349. doi: 10.1196/annals.1297.059

Choi C, Benveniste EN (2004) Fas ligand/Fas system in the brain: regulator of immune and apoptotic responses. Brain Research Reviews 44:65–81. doi: 10.1016/j.brainresrev.2003.08.007

Erten-Lyons D, Jacobson A, Kramer P, and others (2010) The FAS gene brain volume, and disease progression in Alzheimer's disease. Alzheimer's & Dementia 6:118–124. doi: 10.1016/j.jalz.2009.05.663

Edland SD, Vriesé FW-D, Compton D, and others (2003) Insulin degrading enzyme (IDE) genetic variants and risk of Alzheimer's disease: evidence of effect modification by apolipoprotein E (APOE). Neuroscience Letters 345:21–24. doi: 10.1016/s0304-3940(03)00488-9

Aslibekyan S, Vaughan LK, Wiener HW, and others (2016) Linkage and association analysis of circulating vitamin D and parathyroid hormone identifies novel loci in Alaska Native Yup'ik people. Genes & Nutrition. doi: 10.1186/s12263-016-0538-y

Miller JW, Harvey DJ, Beckett LA, and others (2015) Vitamin D Status and Rates of Cognitive Decline in a Multiethnic Cohort of Older Adults. JAMA Neurology 72:1295. doi: 10.1001/jamaneurol.2015.2115

Rajeevan H, Soundararajan U, Kidd JR, and others (2011) ALFRED: an allele frequency resource for research and teaching. Nucleic Acids Research 40:D1010–D1015. doi: 10.1093/nar/gkr924

Wanschers BFJ, van de Vorstenbosch R, Schlager MA, and others (2007) A role for the Rab6B Bicaudal–D1 interaction in retrograde transport in neuronal cells. Experimental Cell Research 313:3408–3420. doi: 10.1016/j.yexcr.2007.05.032

Thyrock A, Ossendorf E, Stehling M, and others (2013) A New Mint1 Isoform but Not the Conventional Mint1, Interacts with the Small GTPase Rab6. PLoS ONE 8:e64149. doi: 10.1371/journal.pone.0064149

Maiese K (2014) Taking aim at Alzheimer's disease through the mammalian target of rapamycin. Annals of Medicine 46:587–596. doi: 10.3109/07853890.2014.941921

Polman JAE, Hunter RG, Speksnijder N, and others (2012) Glucocorticoids Modulate the mTOR Pathway in the Hippocampus: Differential Effects Depending on Stress History. Endocrinology 153:4317–4327. doi: 10.1210/en.2012-1255

Ma T, Hoeffer CA, Capetillo-Zarate E, and others (2010) Dysregulation of the mTOR Pathway Mediates Impairment of Synaptic Plasticity in a Mouse Model of Alzheimer's Disease. PLoS ONE 5:e12845. doi: 10.1371/journal.pone.0012845

Tebbenkamp ATN, Borchelt DR (2010) Analysis of Chaperone mRNA Expression in the Adult Mouse Brain by Meta Analysis of the Allen Brain Atlas. PLoS ONE 5:e13675. doi: 10.1371/journal.pone.0013675